metals

MDPI

Article

The Effect of Corrosion Inhibitors on the Corrosion Behavior of Ductile Cast Iron

Jing Liu [1,2], Bingqin Wang [2], Tianqi Chen [2], Lianjun Hao [2], Jun Wu [1,2,*] and Chao Liu [2,*]

[1] Wuhan Research Institute of Materials Protection Co., Ltd., 126 Bao Feng Erlu, Wuhan 430030, China; liujing04020@163.com
[2] National Materials Corrosion and Protection Data Center, Institute of Advanced Materials & Technology, University of Science and Technology Beijing, Beijing 100083, China; d202110692@xs.ustb.edu.cn (B.W.); tianqichen0709@163.com (T.C.); hlj19861802081@163.com (L.H.)
* Correspondence: cbswuj@sina.com (J.W.); liuchao@ustb.edu.cn (C.L.)

Abstract: Based on actual service environment parameters, this experiment investigated the change in the corrosion rate of nodular cast iron (DCI) in an environment containing organic (triethanolamine phosphate, PTEA) and inorganic (hexametaphosphate, SHMP) inhibitors, and analyzed the effects of both inhibitors and the pH value of the solution on the corrosion behavior of DCI. Additionally, a variable flow rate device was used to conduct immersion tests, enabling the accurate evaluation of the materials' corrosion resistance in an actual service environment. After a certain period, the corrosion of the DCI surface was observed, and the weight loss corrosion rate of the materials was calculated to analyze the differences in corrosion resistance under varying environmental parameters. It was found that the inhibitory effect of both inhibitors on DCI increased with the immersion time, and the inhibitory effect of the SHMP inhibitor was more pronounced under alkaline conditions. Based on the electrochemical and flow rate immersion test results, it can be concluded that, in the solution environment used in this experiment, the inhibitory effect of the SHMP inhibitor on DCI is stronger than that of the PTEA inhibitor.

Keywords: ductile iron; corrosion inhibitor; triethanolamine phosphate (PTEA); sodium hexametaphosphate (SHMP)



Academic Editor: Tomáš Prošek

Received: 13 December 2024
Revised: 9 January 2025
Accepted: 10 January 2025
Published: 15 January 2025

Citation: Liu, J.; Wang, B.; Chen, T.; Hao, L.; Wu, J.; Liu, C. The Effect of Corrosion Inhibitors on the Corrosion Behavior of Ductile Cast Iron. *Metals* **2025**, *15*, 70. https://doi.org/10.3390/ met15010070

Copyright: © 2025 by the authors. Licensee MDPI, Basel, Switzerland. This article is an open access article distributed under the terms and conditions of the Creative Commons Attribution (CC BY) license (https://creativecommons.org/licenses/by/4.0/).

1. Introduction

Cast iron is extensively used in industrial piping due to its excellent castability, wear resistance, and machinability. Ductile cast iron (DCI) is commonly employed in water pipelines due to its enhanced ductility, which results from its internal graphite nodules [1,2]. A cement mortar lining is typically applied inside DCI pipes as a physical barrier to separate water from the cast iron and reduce corrosion [3,4]. However, under actual thermal pipeline conditions, it has been observed that the cement mortar gradually dissolves due to water erosion, or peels off under external forces, leading to secondary pollution [5–7]. In this context, the industry began to promote cementless-lined ductile iron pipes. To prevent the corrosion of ductile iron pipes in thermal pipeline environments, corrosion inhibitors are commonly added. The addition of corrosion inhibitors is the most economical and widely used method [8–11]. The effectiveness of corrosion inhibitors generally depends on the materials, the corrosion environment, and temperature [12]. Therefore, studying the corrosion of DCI in thermal pipeline environments with various corrosion inhibitors is of significant importance.

Corrosion inhibitors can be classified into two categories: organic and inorganic inhibitors, based on their chemical composition. Organic corrosion inhibitors are heterocyclic compounds containing polar functional groups, such as -OH, -COOH, -OCH_3, -$COOC_2H_5$, -NO_2, -NH_2, and -$CONH_2$ [13]. These compounds inhibit corrosion by adsorbing electron-rich polar functional groups and multiple bonds, forming a hydrophobic film on the metal surface. The lone electron pairs of N, O, S, and other atoms in organic inhibitors can form covalent bonds with the empty d orbitals of iron, adsorbing onto the metal surface. These compounds can also act as a barrier film, blocking the anode and cathode active sites or reducing the transmission rate of electroactive substances on the metal surface. PTEA and dimethyl PTEA inhibit the cathodic reaction, thereby slowing down the corrosion of cast iron [14]. E. Naveen et al. [15] used field-emission scanning electron microscopy (TSM-6701F, Japan) and weight loss measurement experiments to study the corrosion inhibition effects of organic inhibitors, including thiourea, glycine, and sodium benzoate, on C45 low-alloy steel pickled in 18% hydrochloric acid. The results showed that the addition of organic corrosion inhibitors to the pickling medium generated nitrides and sulfides, which passivated the low-alloy steel and delayed the corrosion process. Y. Lekbach et al. [16] used weight loss measurement experiments and electrochemical tests to evaluate the effect of methanol extract of rock rose as a corrosion inhibitor for 304L stainless steel in a 1M HCl solution. The results demonstrated that the extract effectively slowed the corrosion of 304L stainless steel, with a corrosion inhibition efficiency of 97.8%.

Inorganic corrosion inhibitors primarily include phosphate (polyphosphate), molybdate, and silicate. Among these, polyphosphate corrosion inhibitors offer the dual advantages of corrosion and scale inhibition. The addition of a small amount of polymeric phosphate (such as SHMP) to a solution enables it to react with cations, such as calcium, magnesium, and iron, forming insoluble complexes that create a protective film on the metal surface, thereby inhibiting the corrosion process. However, excessive polyphosphate concentrations should be avoided, as they can lead to the formation of water-soluble compounds [17]. Phosphate ions can convert $Fe(OH)_2$ into $FePO_4$ during corrosion, adhering to the surface of the iron matrix to form a protective film that hinders the corrosion process [18]. Ambrish Singh et al. employed electrochemical impedance spectroscopy (EIS) [19], potentiodynamic polarization (PDP), density functional theory (DFT), and molecular dynamics simulations (MDS) to investigate the corrosion inhibition effect of the green composite corrosion inhibitor PCP on N80 steel bars in 15% hydrochloric acid. The study found that PCP could delay the corrosion process of steel bars by inhibiting the diffusion of corrosive substances at a concentration of 400 mg/L, with an efficiency of 98.4%. In an electrolyte system with 3.5 wt.% NaCl solution as the electrolyte, Chen Shuqing [20] employed an open circuit potential–time curve (OCP) and a polarization steady-state curve (Tafel) to select the appropriate corrosion inhibitor to mitigate the non-discharging corrosion of an aluminum anode. Electrochemical impedance spectroscopy (EIS), scanning electron microscopy (SEM), energy-dispersive spectroscopy (EDS), and X-ray photoelectron spectroscopy (XPS) were employed to investigate the corrosion inhibition mechanism and the film formation morphology of the inhibitor on the aluminum electrode surface. The results demonstrated that sodium metavanadate and sodium oleate were combined in a specific proportion. The resulting compound corrosion inhibitor formed a protective film on the surface of the aluminum anode, effectively inhibiting corrosion.

At present, limited studies have investigated the corrosion inhibition mechanisms of PTEA and SHMP on ductile cast iron (DCI). K. T. Kim's team [21] found that triethanolamine (TEA) preferentially adsorbs onto the graphite spheres in DCI. When TEA is present in sufficient amounts, it can cover the surface of DCI, reducing the galvanic corrosion between the graphite and the matrix, while hindering the contact between the corrosive solution and

the DCI surface, thereby achieving a corrosion inhibition effect. Harish Kumar's team [22] reported that SHMP was found to form a stable cage complex with Fe^{2+} in steel, which adsorbs at the anode and inhibits the anodic reaction. Their study also revealed that temperature significantly affects the corrosion inhibition efficiency of SHMP. However, research remains lacking on the effects of PTEA and SHMP corrosion inhibitors on the corrosion behavior of DCI under high-temperature, varying pH, and dynamic immersion conditions.

Therefore, to investigate the effects of PTEA and SHMP corrosion inhibitors on the corrosion resistance of ductile iron pipes, electrochemical test samples of ductile iron pipes were prepared, and electrochemical tests were conducted in a solution containing PTEA and SHMP corrosion inhibitors. The variation in electrochemical parameters, such as corrosion potential and corrosion current density, due to the corrosion inhibitors was analyzed using electrochemical impedance spectroscopy and potentiodynamic polarization curves. The phase structure and composition of the material surface were examined using scanning electron microscopy and laser confocal scanning microscopy (LSCM). The corrosion resistance of ductile iron pipes was evaluated in environments containing varying types of corrosion inhibitors.

2. Experimental Program

2.1. Microstructure and Morphology Observations

The ductile cast iron (DCI) samples were cut to dimensions of 10 mm × 10 mm × 5 mm and ground sequentially using sandpapers with grits of 240#, 400#, 800#, 2000#, 3000#, and 5000#. Subsequently, they were polished using a 1 μm diamond suspension. The final step involved ultrasonic cleaning with anhydrous ethanol, followed by examination of the microscopic morphology of the ductile cast iron using a scanning electron microscope (FEI Quanta 250, FEI Company, Hillsboro, OR, USA) at a working voltage of 20 kV.

2.2. Electrochemical Testing

According to the pipeline operation environment data, the following test environments were selected for electrochemical analysis and testing. The test conditions are shown in Table 1. The solution hardness was adjusted using $CaCO_3$, while the concentration of Cl^- was adjusted using NaCl. The same batch of immersion was performed using a large 8-hole water bath with Sedlis electrothermal digital display (Sedlis Experimental Analysis Instrument Manufacturing Factory, Tianjin, China) constant temperature. During electrochemical testing, a small single-hole water bath with Sedlis electrothermal digital display constant temperature was used for electrochemical measurements at a constant temperature. The temperature control accuracy of the water bath was 0.5 °C, while the temperature control range was 5–100 °C, with a power of 300 W. The electrochemical tests were conducted under experimental cycles of no immersion, 3 days of immersion, and 10 days of immersion, respectively.

Table 1. Proposed test environment for testing.

Environment	Hardness (mg/L)	Cl^- (mg/L)	Water Temperature (°C)	pH	Corrosion Inhibitor Type
1	80	20	90	7	No additions
2					PTEA
3					SHMP
4	80	20	90	11	No additions
5					PTEA
6					SHMP

The electrochemical measurements were performed using a PARSTAT 4000A electrochemical workstation (Princeton Applied Research, Oak Ridge, TN, USA). All electrochemi-

cal tests were conducted using the classic three-electrode system, in which a platinum plate was used as the counter electrode, Ag/AgCl (SSCE) was used as the reference electrode, and ductile iron samples were employed as the working electrode. The electrochemical samples were sealed with high-temperature-resistant epoxy resin, having an exposed area of 1 cm^2. The exposed surface was polished using 240# to 2000# silicon carbide sandpaper. Before the electrochemical experiment, the open circuit potential (OCP) was measured for at least 30 min until a stable state was reached. When the dynamic polarization curve was measured, the scanning rate was 0.333 mV/s, and the scanning potential range was from −0.5 V vs. OCP to −0.8 V vs. OCP. During the electrochemical impedance spectroscopy (EIS) measurements, the scanning frequency ranged between 100 kHz and 0.01 Hz, with a perturbation voltage of 10 mV. All measurements were carried out at least three times to ensure reproducibility. More experimental details can be found in our previous study [23]. The concentrations of PTEA phosphate inhibitor and SHMP inhibitor were both 200 ppm.

2.3. Corrosion Kinetics Analysis

In order to accurately evaluate the corrosion resistance of materials in an actual service environment, this work was conducted using a variable flow rate device for the immersion test. The flow rate of the solution was set at 1.25 m/s, and the weight loss corrosion rate of the materials was calculated after a certain period (immersion for 5 days). The corrosion rate (V_{corr}, in millimeters per year, mm/a) of ductile iron specimens is determined by the weight loss before and after immersion, as shown in Equation (1) [24]:

$$v = \frac{\Delta W \times 365 \times 10}{S \times T \times \rho} \quad (1)$$

where Δw is the weight loss before and after immersion, g; S represents the exposed area of the samples in the immersion experiment, cm^2; T denotes the immersion time, d; and ρ is the density of ductile iron, 7.3 g/cm^3.

Subsequently, scanning electron microscopy (FEI Quanta 250, FEI Company, Hillsboro, OR, USA) was employed to characterize the corrosion morphology of samples before and after rust removal after the flow immersion test, employing an accelerating voltage of 20 kV. After rust removal, the depth of corrosion pits on the surface of the sample was measured and quantified using a confocal laser scanning microscope (CLSM VK-9700, KEYENCE, Osaka, Japan). The specific test environment is shown in Table 1.

3. Experimental Results

3.1. Characterization of the Microstructure of the Material

The surface morphology of the samples was analyzed using an SEM. The SEM image of ductile cast iron (DCI) is shown in Figure 1. From the two surface morphology images, it can be observed that the graphite particles exhibit a regular spherical or nearly spherical shape and are evenly distributed across the surface of the sample.

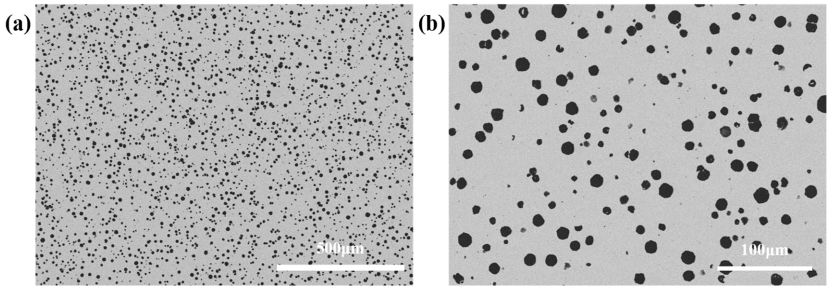


Figure 1. Surface morphology of ductile iron: (**a**) low magnification view; (**b**) high magnification view.

3.2. Electrochemical Test Results

3.2.1. Open Circuit Potentials (OCPs)

In Figure 2a–c, the OCP test results for the DCI immersed in the solution environments described in Table 1 for 0, 3, and 10 days are presented. Table 2 summarizes the OCP values, as represented in Figure 2d. The OCP test results indicate that when the DCI is exposed to environment 1 (neutral environment without a corrosion inhibitor), the initial OCP is the lowest. After 3 and 10 days of immersion, the OCP remains nearly constant, suggesting that a relatively stable corrosion product film likely formed on the surface of the DCI after 3 days. When the DCI is exposed to environment 2 (neutral PTEA inhibitor environment), the initial OCP is higher than that in the environment without an inhibitor. After 3 days of immersion, the OCP increases, and after 10 days, it slightly decreases, but both values are higher than the OCP in environment 1. When the DCI is exposed to environment 3 (neutral SHMP corrosion inhibitor environment), the OCP increases over time, reaching its maximum value on the 10th day, indicating that the cast iron surface develops a certain level of corrosion resistance at this point.

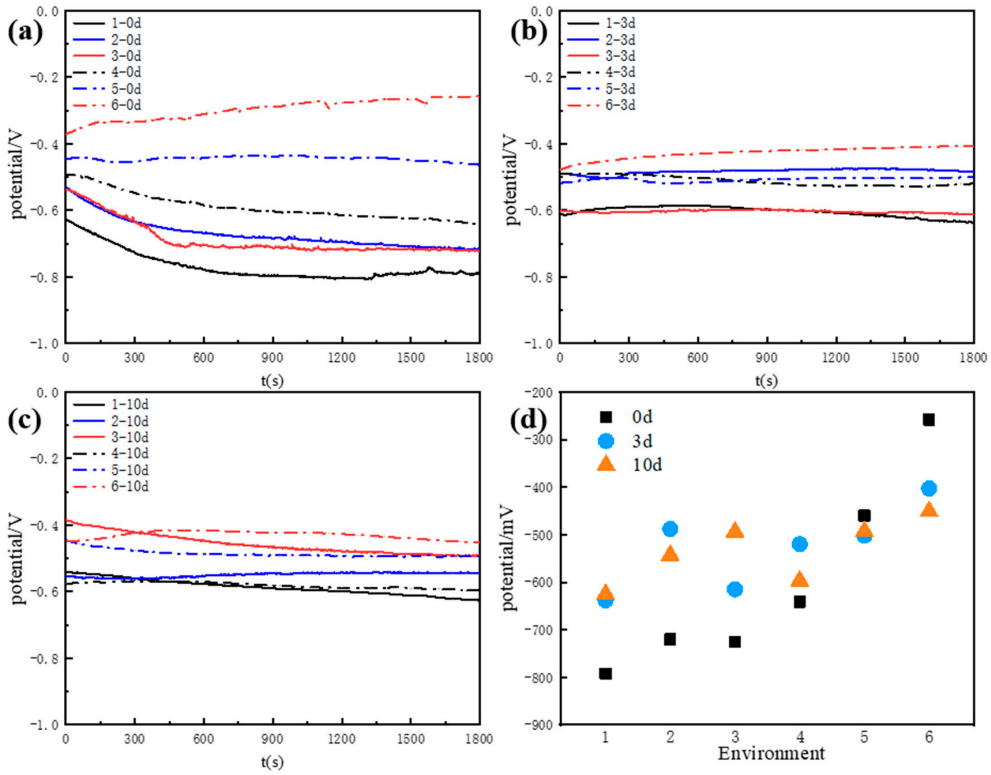


Figure 2. OCP test and results of DCI under environments in Table 1: (**a**) soaking for 0 days; (**b**) soaking for 3 days; (**c**) soaking for 10 days; and (**d**) OCP value.

Table 2. OCP of ductile iron in eight environments in Table 1.

Environment	OCP/mV		
	0 d	**3 d**	**10 d**
1	−792	−638	−625
2	−720	−488	−543
3	−726	−615	−494
4	−641	−520	−597
5	−460	−502	−493
6	−258	−403	−451

In environment 4 (alkaline environment without a corrosion inhibitor), the initial OCP is significantly higher compared to the neutral environment. As the immersion time increases, the OCP initially increases and then decreases. This may be due to the passive film that forms easily on the surface of DCI in an alkaline environment but fails to remain stable under the influence of corrosive ions and a high temperature. When the DCI is exposed to environment 5 (alkaline PTEA corrosion inhibitor environment), the initial OCP increases significantly, and the OCP slightly decreases after 3 and 10 days of immersion, indicating that the PTEA corrosion inhibitor in an alkaline environment effectively forms a protective film on the surface of the cast iron and demonstrates good stability. In environment 6 (alkaline SHMP corrosion inhibitor environment), the initial OCP is the highest, and it decreases after immersion for 3 and 10 days, but remains higher than the OCP in all the other environments, indicating the pronounced corrosion inhibition effect of the SHMP corrosion inhibitor in alkaline environments, which effectively inhibits the electrochemical reaction of cast iron. In general, the presence of corrosion inhibitors increases the OCP of cast iron, and corrosion inhibitors in alkaline environments show the best corrosion inhibition effects, with SHMP in the alkaline environment exhibiting the most significant corrosion resistance.

3.2.2. Polarization Curves

Figure 3a–c present the electrochemical polarization curve test results for the DCI immersed in the six solution environments, as listed in Table 1, for 0, 3, and 10 days. Table 3 summarizes the corrosion potential (E_{corr}) and corrosion current density (i_{corr}), which are shown in Figure 3d. Figure 3a shows that the anode of the DCI in a neutral environment exhibits a clear activation process. When an inhibitor is added, the cathodic corrosion rate decreases, indicating that the addition of the inhibitor slows down the electrochemical cathodic reaction, thereby reducing the overall corrosion rate. The initial corrosion inhibition effect of SHMP in a neutral environment is more pronounced. In an alkaline environment, the anode of the ductile iron still exhibits an activation process in the solution without a corrosion inhibitor, but the corrosion potential increases significantly, and the i_{corr} decreases from 41.4 $\mu A/cm^2$ to 8.5 $\mu A/cm^2$. In both solution environments containing corrosion inhibitors, a passivation zone forms, and the passivation potentials (E_p) in the SHMP and PTEA environments are −332 mV and −657 mV, respectively, with passivation current densities (i_{ps}) of 1.6 $\mu A/cm^2$ and 6.3 $\mu A/cm^2$, respectively. This suggests that in an alkaline environment, a corrosion inhibitor has a greater effect on the rate of the electrochemical anodic reaction, possibly due to the formation of a protective film between the corrosion inhibitor and the cast iron surface, which prevents further interaction between the cast iron and the corrosive solution.

As shown in Figure 3b, in the neutral environment without an inhibitor, the slope of the anode region of the polarization curve shifts significantly, indicating an enhancement of the anodic activation corrosion process on the cast iron surface, which leads to a decrease in the E_{corr} from −759 mV (0 d) to −928 mV, while the i_{corr} significantly increases from 41.4 $\mu A/cm^2$ (0 d) to 297 $\mu A/cm^2$. After the inhibitor is added, the polarization curve shifts overall to the upper left, indicating an increase in the corrosion potential. Meanwhile, the change in the slope of the anode region suggests a decrease in the i_{corr}, reflecting the corrosion inhibition effect. In the alkaline environment with the SHMP inhibitor, a clear passivation zone forms, with the i_p at 10.2 $\mu A/cm^2$. In the other two environments, the polarization curve shows minimal changes, although the i_{corr} decreases slightly in the alkaline environment. Figure 3c shows that in the neutral environment without an inhibitor, the E_{corr} decreases to −986 mv and the i_{corr} increases to 776 $\mu A/cm^2$, whereas the i_{corr} remains relatively unchanged in the environment with the PTEA inhibitor. In the SHMP

inhibitor environment, the polarization curve exhibits passivation–depassivation behavior, with a trend toward passivation. The changes in the corrosion potential and corrosion current clearly demonstrate a corrosion inhibition effect. In the alkaline environment, the polarization curve with the SHMP inhibitor presents a distinct passivation zone, with a passivation current density (i_p) of 17.3 μA/cm^2. In the other two environments, the polarization curve shows minimal changes, although the i_{corr} decreases slightly in the alkaline environment.

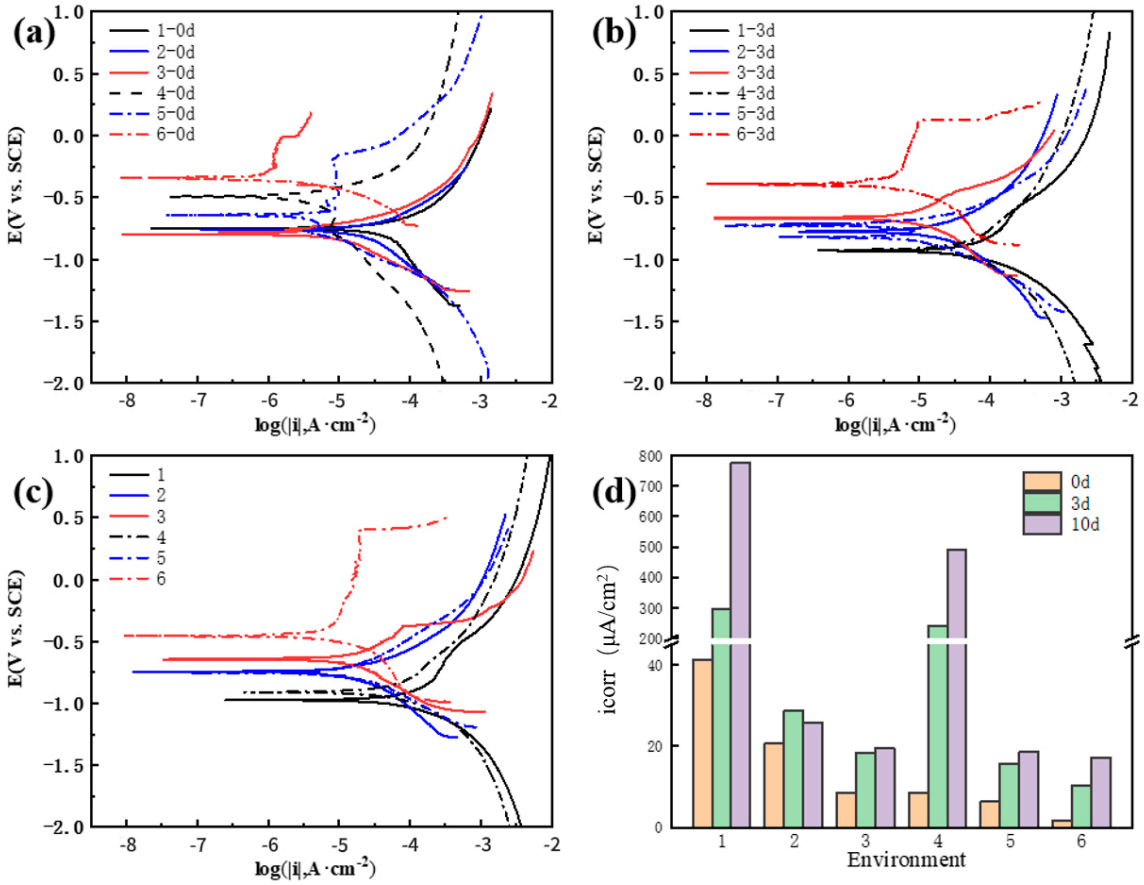


Figure 3. Electrochemical polarization curve test and results of DCI under six environments in Table 1: (**a**) soaking for 0 days; (**b**) soaking for 3 days; (**c**) soaking for 10 days; and (**d**) statistical results of the corrosion current density.

Table 3. E_{corr} and i_{corr} for ductile iron in six environments.

Environment	E_{corr} (mV)			i_{corr} (μA/cm^2)		
	0 Days	3 Days	10 Days	0 Days	3 Days	10 Days
1	−759	−928	−986	41.4	297	776
2	−761	−783	−762	20.8	28.8	25.7
3	−775	−666	−641	8.5	18.2	19.4
4	−498	−917	−894	8.5	239	489
5	−657	−738	−774	6.3	15.8	18.6
6	−332	−379	−448	1.6	10.2	17.3

In all the environments, the i_{corr} generally increases after 3 days of immersion, as shown in Table 3. This may result from the dissolution of active centers (e.g., defects) on the cast iron surface, allowing the corrosive solution to penetrate the protective film and

form a corrosion couple at the interface between the steel substrate and the protective film. As the immersion time extends to 10 days, the surface protective film becomes more stable, leading to a lower corrosion rate for the cast iron.

According to ASTM G102-23 [25], Faraday's law suggests that the corrosion current density can be converted into the corrosion rate, with its magnitude serving as a significant indicator of the corrosion kinetic process, as shown in Equation (2) [26]:

$$CR = \frac{3.27 \times 10^{-3} i_{corr} E_w}{\rho} \quad (2)$$

where 3.27×10^{-3} is the conversion factor, i_{corr} is the corrosion current density, E_w is the equivalent weight of the metal, and ρ is the metal's density.

The corrosion inhibition efficiency of an inhibitor can be evaluated based on the i_{corr} ratio. Table 4 indicates that the SHMP corrosion inhibitor exhibits superior corrosion inhibition in alkaline environments, as evidenced by the low i_{corr} values and distinct passivation zones observed in the polarization curves.

Table 4. Corrosion inhibition efficiency of ductile iron of two corrosion inhibitors.

Environment	Corrosion Inhibitors	Corrosion Inhibition Efficiency		
		0 Days	3 Days	10 Days
pH = 7	PTEA	51.8%	90.3%	96.7%
	SHMP	79.5%	93.9%	97.5%
pH = 11	PTEA	25.9%	93.4%	96.2%
	SHMP	81.2%	95.7%	96.5%

The comprehensive polarization curve test results indicate that both inhibitors exert a noticeable inhibitory effect on the corrosion of the DCI. The inhibitory effect of the PTEA inhibitor is stable, effectively reducing the corrosion rate of the DCI during the electrochemical reaction in both the neutral and alkaline environments. However, the SHMP corrosion inhibitor is more effective than the PTEA inhibitor at inhibiting DCI corrosion, particularly in alkaline environments.

3.2.3. EIS

Figure 4 presents the electrochemical impedance spectra of the DCI in the six environments listed in Table 1. As shown in Figure 4, the impedance spectrum of the DCI consists of a high-frequency capacitive arc and a medium-to-low frequency capacitive arc (Figure 4a–c). The high- and intermediate-frequency capacitive arcs are smaller than the low-frequency arc, suggesting that the protective film formed on the surface of the cast iron inhibits solution penetration and hinders the electrochemical reactions between the cast iron surface and the solution. This indicates that the resistance between the cast iron surface and the protective film interface is the primary controlling factor. As observed in Figure 4a, the impedance curves are generally dispersed, forming capacitive reactance arcs. On one hand, the similar shape suggests that the inhibitor does not alter the electrochemical reaction mechanism at the metal/solution interface. On the other hand, the flat capacitive arc suggests a significant dispersion effect at the steel/solution interface. Under the same corrosion medium, the arc radius of the DCI containing the SHMP inhibitor is the largest, indicating that the addition of an inhibitor, particularly SHMP, enhances the blocking effect on the interface electrochemistry and significantly improves the corrosion resistance.

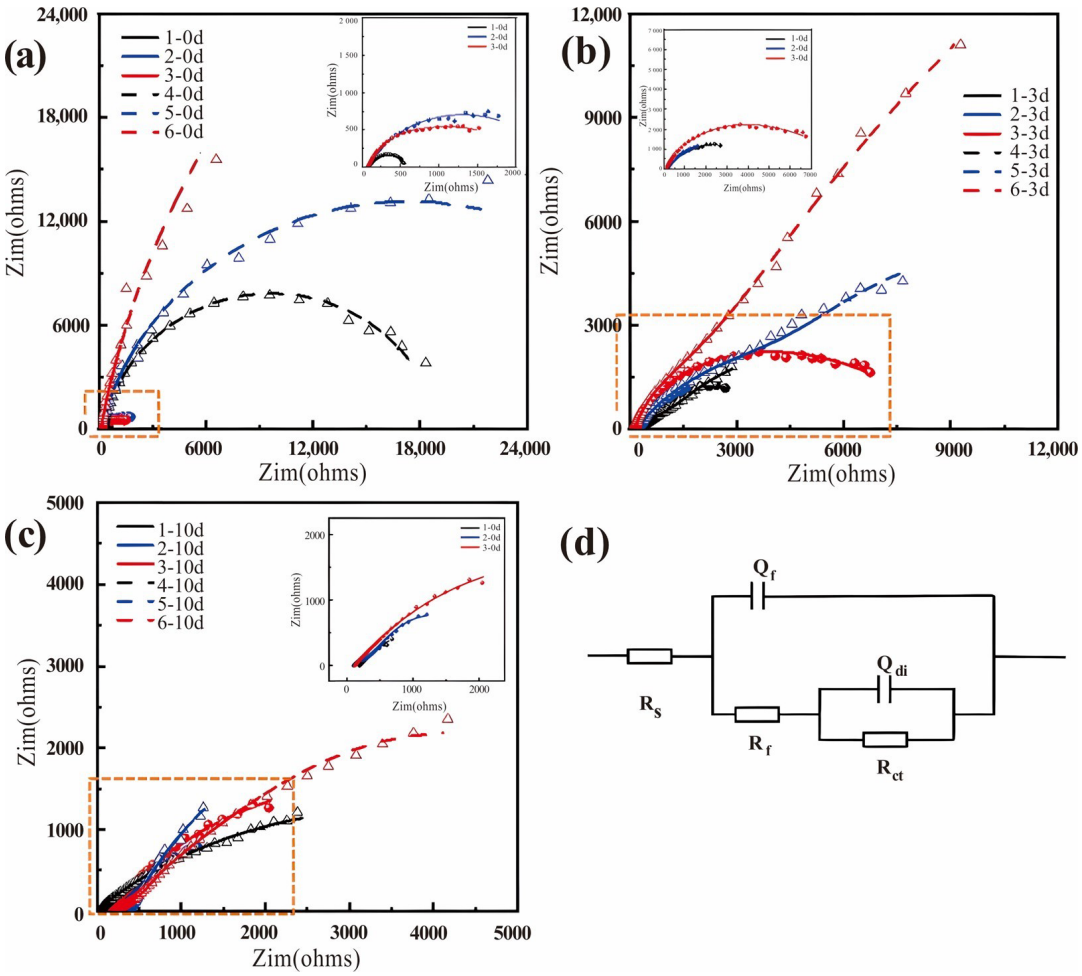


Figure 4. Electrochemical impedance spectroscopy test and results for DCI under 6 environments in Table 1: (**a**) immersion for 0 days; (**b**) soaking for 3 days; (**c**) soaking for 10 days; and (**d**) EIS-fitted circuit diagram.

The corresponding Bode diagram is shown in Figure 5. A high-frequency capacitance loop forms at the interface between the protective film and the solution, while a low-frequency capacitance loop forms at the interface between the protective film and the cast iron matrix. In the Bode diagram for environments containing corrosion inhibitors, the phase angle is higher in the middle- and low-frequency ranges, indicating the presence of a protective film. This indicates that the protective film formed exhibits the strongest corrosion inhibition effect. In the three neutral environments, the impedance value initially increased and then decreased with extended immersion time. This may have been due to the formation of a relatively stable protective film during the early immersion stage of the ductile iron. However, under the combined influence of high temperature and Cl^-, the passivation film on the surface of the ductile iron dissolved, leading to further corrosion of the steel matrix.

In the three alkaline environments, the initial impedance value was the highest, indicating that the alkaline environment accelerated the formation of a protective film on the surface of the ductile iron. After 3 days of immersion, the R_p decreased significantly, possibly because the Cl^- disrupted the stability of the protective film, increasing the active sites on the cast iron surface at high temperatures and accelerating the corrosion process. Notably, the impedance value of the PTEA corrosion inhibitor changed little in both the neutral and alkaline environments, indicating stronger stability.

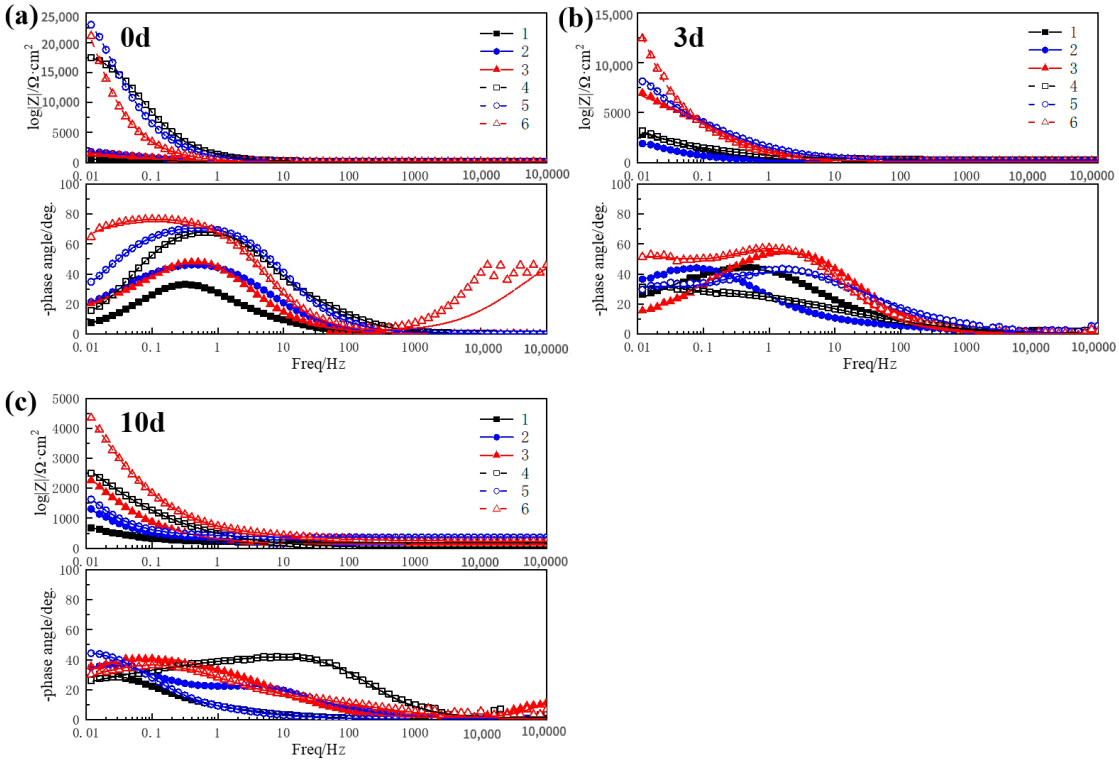


Figure 5. Bode diagram and results for DCI under 6 environments in Table 1: (**a**) immersion for 0 days; (**b**) soaking for 3 days; and (**c**) soaking for 10 days.

Considering the physical and chemical processes at the interface, ZsimpWin software (version is 3.6) was used to analyze the impedance data, and the equivalent circuit shown in Figure 4d was employed for the fitting. The repeatability between the fitted curve and the measured data is high, indicating the validity of the equivalent circuit. The corresponding fitting results are provided in Table 5. Specifically, Rs represents the solution resistance, R_f and Q_f represent the corrosion product film resistance and the corresponding constant phase angle element (CPE), and R_{ct} and Q_{dl} represent the charge transfer resistance and double-layer capacitance at the steel/solution interface, respectively. Due to the dispersion effect, a constant phase angle element is used to replace the pure capacitance. The CPE can be defined by the following formula:

$$Z_{CPE} = \frac{1}{Y_0(j\omega)^n} \quad (3)$$

where Y_0 is the modulus of the CPE, ω is the angular frequency, j is the imaginary unit ($j^2 = -1$), and n is the dispersion effect index, reflecting the non-uniformity of the electrode surface. When n = 0, the CPE represents resistance; when n = −1, it represents inductance; and when n = 1, it represents capacitance.

The charge transfer resistance (R_{ct}) increased significantly in the two environments containing corrosion inhibitors. When immersed in a solution with pH = 11 for 3 days, the R_{ct} increased from 7.75 kΩ·cm^2 without a corrosion inhibitor to 12.27 kΩ·cm^2 with the PTEA corrosion inhibitor. The R_{ct} obtained by immersion in a solution with the SHMP corrosion inhibitor was the largest, 17.8 kΩ·cm^2. The SHMP corrosion inhibitor adsorbed onto the surface of the DCI to form an inhibition film, increasing the difficulty of charge transfer, which is consistent with the literature findings. The polarization resistance ($R_P = R_{ct} + R_f$) reflects the key indicators of corrosion resistance, the R_P values in six environments are shown in Figure 6.

Table 5. Fitted values of electrochemical impedance spectra of ductile iron for six environments in Table 1.

Immersion Time	Environment	R_s	Q_f		R_f	Q_{dl}		Rct
		Ω·cm²	Y_0 (10^{-3} $\Omega^{-1}\cdot cm^{-2}\cdot s^n$)	n	Ω·cm²	Y_0 (10^{-3} $\Omega^{-1}\cdot cm^{-2}\cdot s^n$)	n	Ω·cm²
0 days	1	90.19	1.90	0.79	96.1	1.30	0.80	392.6
	2	79.68	0.32	0.98	27.1	1.12	0.60	2524
	3	86.09	1.29	0.83	111.7	5.76	0.65	981.3
	4	155	0.07	0.90	202	0.08	0.87	18,790
	5	119	0.20	0.87	230.5	0.02	0.65	37,690
	6	100	0.01	0.73	103.1	0.44	0.89	89,930
3 days	1	102.2	0.08	0.59	258.7	0.08	0.94	4426
	2	131.8	0.84	0.60	83.7	1.38	0.73	4297
	3	127	0.14	0.83	158.7	0.12	0.38	8940
	4	251.3	0.79	0.44	542.8	1.03	0.89	7744
	5	191.1	0.21	0.60	800.1	1.19	0.85	12,270
	6	133.1	0.23	0.81	4576	0.34	0.73	17,800
10 days	1	159.9	4.99	0.58	173.7	3.31	0.79	1297
	2	101.1	0.86	0.63	330.5	3.86	0.72	2755
	3	121.5	1.66	0.83	120.6	1.49	0.58	6108
	4	28.7	0.80	0.42	43.8	0.06	0.86	7026
	5	272.2	2.88	0.63	396.1	1.23	0.91	12,380
	6	225.8	0.31	0.53	414.2	0.44	0.71	12,660

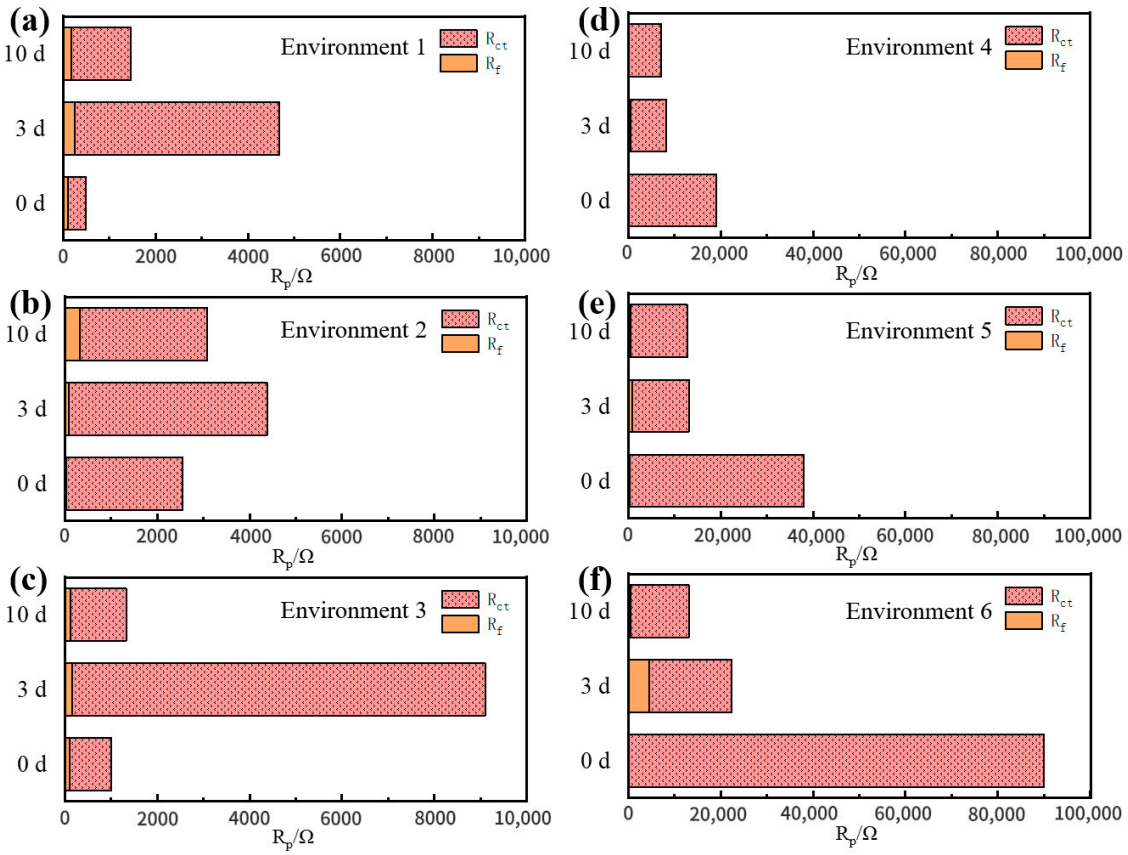


Figure 6. Fitted values for R_p of electrochemical impedance spectra of ductile iron for six environments in Table 1.

In environment 1, the R_P value initially increased and then decreased with prolonged immersion time. This suggests that corrosion products formed on the surface of the cast iron after 3 days of immersion, where they were deposited at active sites, hindering the charge transfer process. However, under the action of corrosive ions, the surface of the cast iron was further dissolved, leading to a decrease in the impedance value. The trend of the

R_P in environment 2 was similar to that in environment 1, but the R_P was slightly higher after 10 days of immersion. This suggests that PTEA provides poor protection for cast iron in a neutral environment.

In environment 3, the R_P increased with immersion time, significantly hindering the charge transfer process between the protective film and the cast iron substrate. This indicates that SHMP forms a relatively stable protective film on the surface of cast iron in a neutral environment. In environment 4, the R_P of the cast iron was significantly higher than in environment 1. The alkaline environment promoted the formation of a passivation film on the surface of the cast iron. With prolonged immersion time, the R_P first increased and then decreased significantly. This may have been due to the breakdown of the surface passivation film under the high-temperature alkaline conditions, with corrosive ions gathering at the active sites on the cast iron surface, accelerating the charge transfer process.

In environment 5, PTEA significantly hindered the electrochemical reaction process on the surface of the cast iron during the initial stage of immersion. However, after 10 days of immersion, the R_P decreased, but remained higher than in the environment without a corrosion inhibitor. In environment 6, under the action of SHMP, the SHMP corrosion inhibitor formed a protective film on the surface of the cast iron during the initial stage of immersion, preventing the corrosive solution from contacting the cast iron surface. As the immersion time increased, the R_P decreased, but the impedance value remained high, indicating that SHMP forms a stable protective film on the surface of cast iron in an alkaline environment, which hinders the electrochemical reaction process. In general, the relationship of the R_P is as follows: SHMP inhibitor > PTEA inhibitor > no inhibitor. The addition of an inhibitor interferes with the charge transfer process at the interface, thereby improving the corrosion resistance of DCI.

3.3. Flow Rate Immersion Experiments

To study the corrosion kinetics and the evolution of the corrosion morphology of ductile iron materials under actual service conditions, an immersion test was conducted using a variable flow rate device (1.25 m/s). After 120 h, the weight loss corrosion rate of the materials was measured, and the surface morphology of the derusted ductile iron samples was observed to analyze the differences in the corrosion resistance. The specific experimental conditions are shown in Table 1. As shown in Figure 7, the macromorphology of the DCI surface before and after rust removal, following a 120 h flow rate immersion test under the conditions specified in Table 1, is presented. After rust removal, the depth of the corrosion pits on the surface of the sample was measured and quantified using a confocal microscope. The confocal image is shown in Figure 8. The weight loss corrosion rate of the sample was calculated after rust removal, the results are presented in Figure 9 and Table 6. To investigate the protective properties of the rust layers formed in different environments, scanning electron microscopy (SEM) was employed to characterize the corrosion morphology of the samples before and after rust removal after the flow immersion test, as shown in Figures 10 and 11.

Table 6. Weight loss corrosion rate (10 d) of DCI under 6 environments in Table 1.

Environment	1	2	3	4	5	6
Weight loss corrosion rate (mm/a)	3.542	2.984	2.371	1.353	0.954	0.135

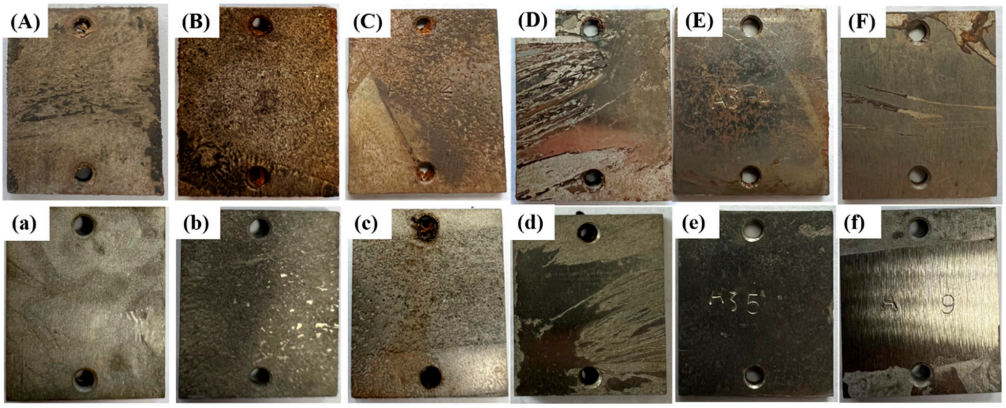


Figure 7. Corrosion morphology of samples after flow rate immersion test: (**A**–**F**) morphology of DCI before rust removal, corresponding to environments 1~6 in Table 1, respectively; (**a**–**f**) morphology of DCI after rust removal, corresponding to environments 1~6 in Table 1.

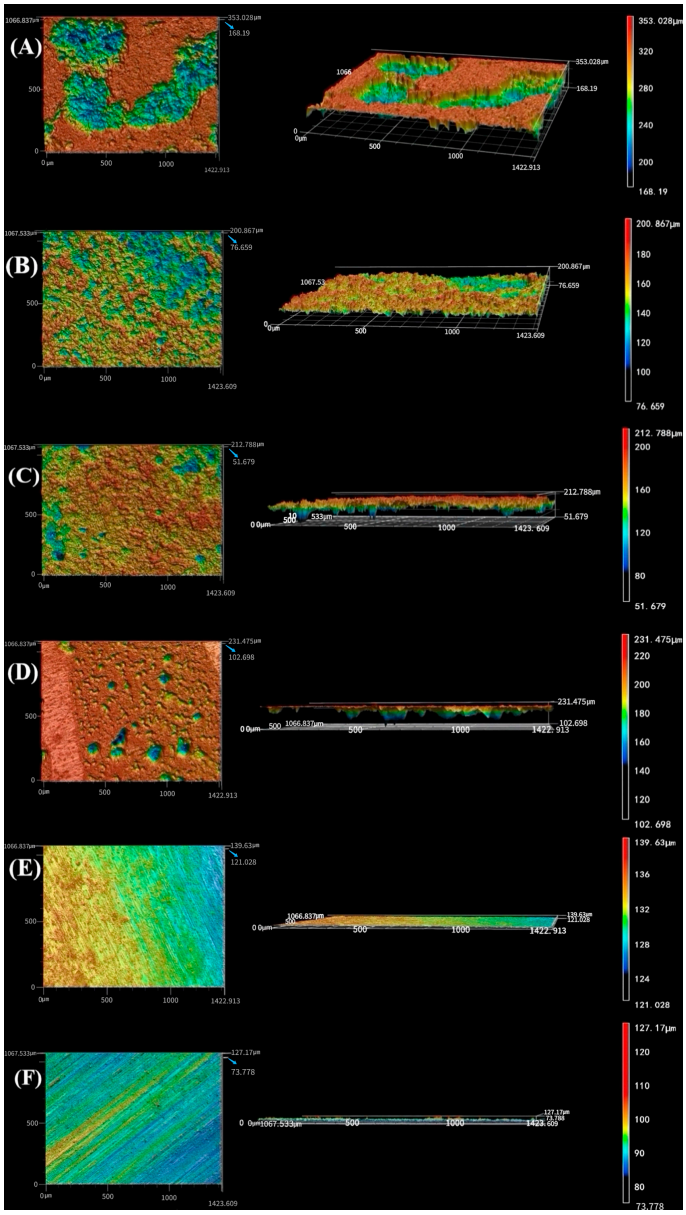


Figure 8. Confocal image of flow rate immersion test sample after rust removal: (**A**–**F**) surface-treated ductile iron corresponds to environments 1~6 in Table 1, respectively.

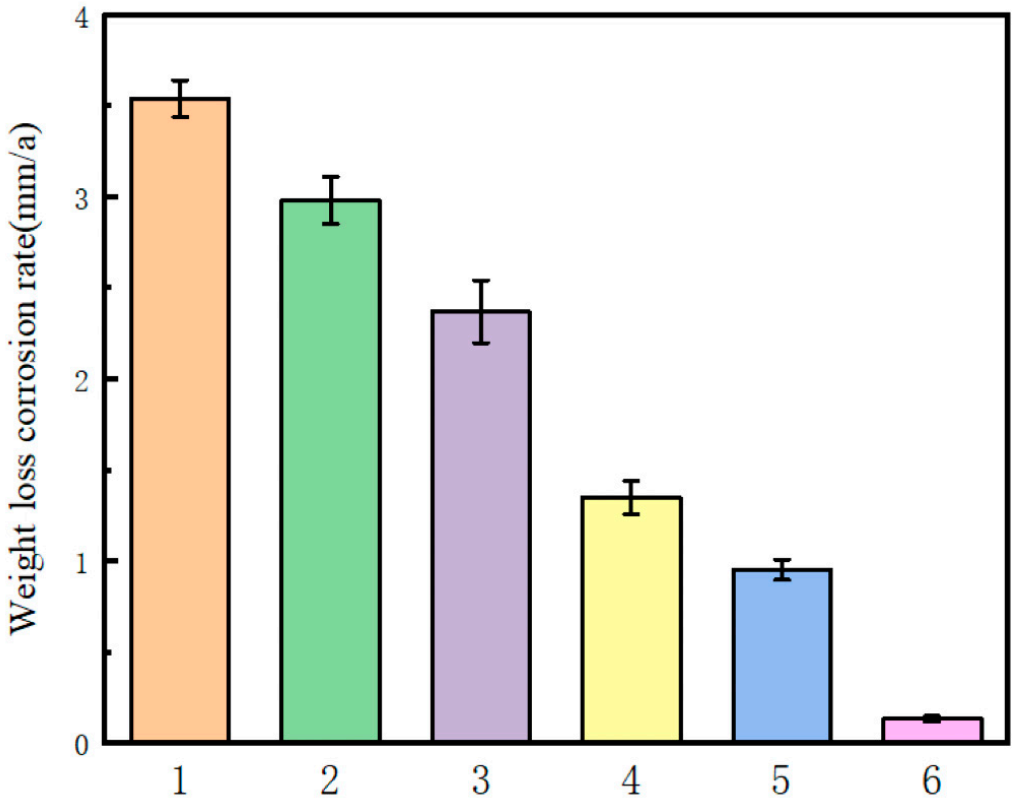


Figure 9. Histogram of weightless corrosion rates for flow rate immersion experiments.

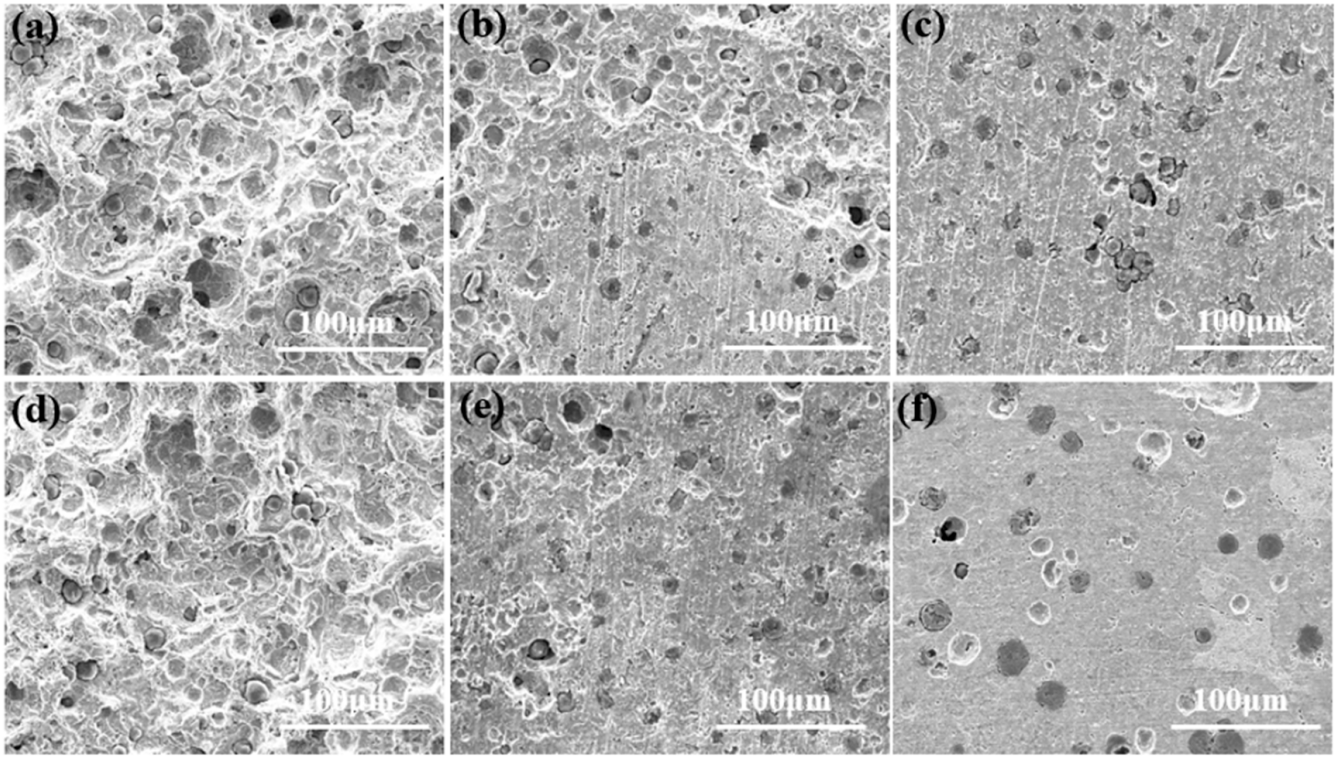


Figure 10. Corrosion SEM morphology of sample after flow rate immersion test: (**a**–**f**) morphology of DCI before rust removal, corresponding to environments 1~6 in Table 1, respectively.

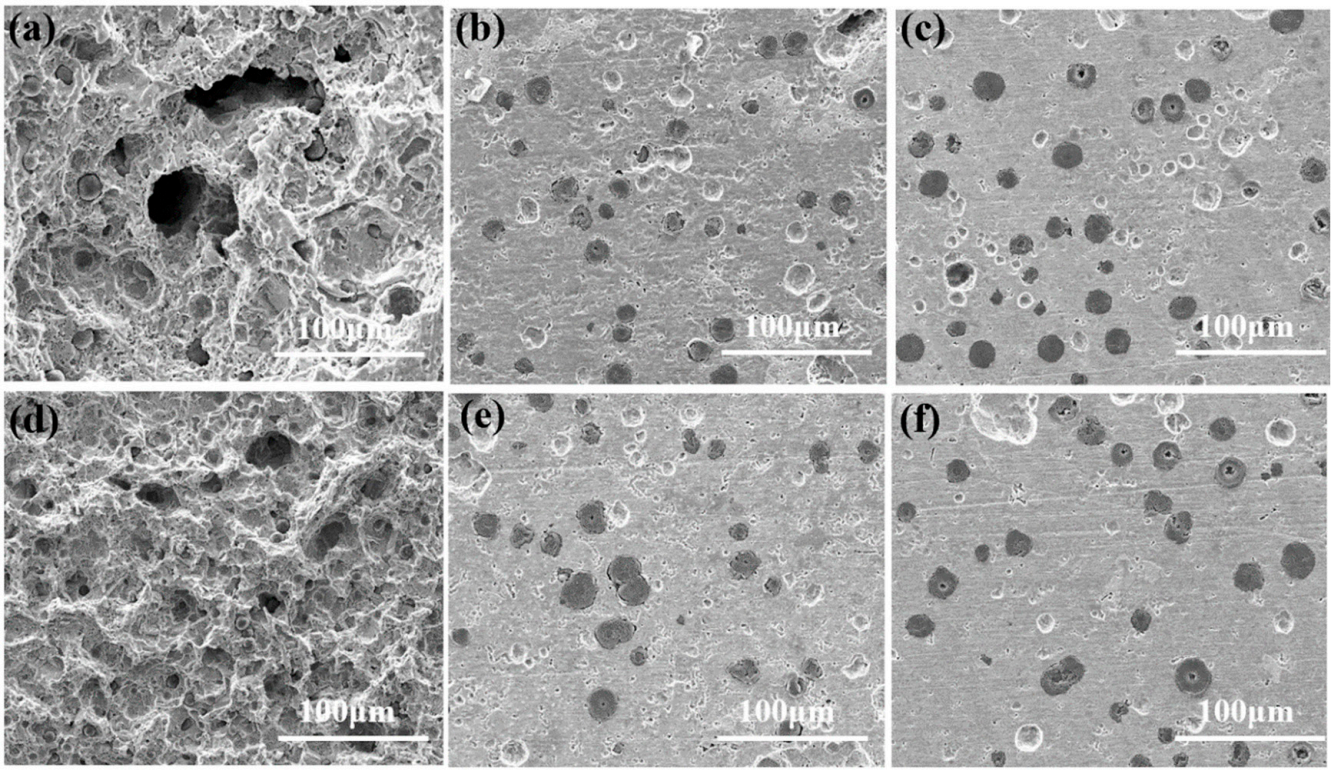


Figure 11. Corrosion SEM morphology of samples after flow rate immersion test: (**a**–**f**) morphology of DCI after rust removal, corresponding to environments 1~6 in Table 1, respectively.

Figure 7A–F illustrate the corrosion morphology of the unblasted ductile iron samples. Before rust removal, the corrosion morphology in the alkaline environment is more uniform than that in the neutral environment, and the corrosion inhibition effect is more pronounced in the alkaline environment upon the addition of inhibitors. Figure 7a–f present the corrosion morphology of the samples following rust removal. Following rust removal, the surface of the ductile iron in the alkaline environment is smoother than that in the neutral environment, and the corrosion inhibition effect is further enhanced with the addition of inhibitors, resulting in a more uniform surface. Overall, regardless of whether it is in a neutral or alkaline environment, ductile iron with an SHMP inhibitor exhibits a more uniform and smoother corrosion morphology both before and after rust removal compared to a PTEA inhibitor, with the SHMP inhibitor demonstrating the most significant effect in an alkaline environment.

The corrosion degree of ductile iron in various environments (see Table 1) is further examined using LSCM. As shown in Figure 8A–C, all the samples are exposed to a neutral environment. The maximum depth of pitting corrosion in the sample without any inhibitor reaches 353.028 μm, while the maximum depths of pitting in the samples with PTEA and SHMP are 200.867 μm and 212.788 μm, respectively. Figure 8D–F display the corrosion characteristics in an alkaline environment. Compared to the neutral environment, the maximum depth of pitting corrosion in ductile iron is significantly reduced in the alkaline environment. The maximum depth of pitting in the sample without any inhibitor decreases to 231.475 μm, while the maximum depths in the samples with PTEA and SHMP are reduced to 139.63 μm and 127.17 μm, respectively. From the changes in the maximum depth of pitting corrosion, it can be concluded that SHMP exhibits a more significant corrosion inhibition effect on ductile iron in an alkaline environment.

The weight loss corrosion rate of the DCI was calculated after the flow rate immersion test, and the results are presented in Figure 9 and Table 6. The weight loss corrosion rate

of the DCI in the alkaline environment was significantly lower than that in the neutral environment. Among them, the SHMP inhibitor exhibited the strongest corrosion inhibition effect, which is consistent with the electrochemical test results.

As shown in Figure 10a–c, in a neutral environment, the surfaces of the samples without a corrosion inhibitor exhibit numerous corrosion pits and rough corrosion products, indicating the most severe corrosion. Following the addition of the PTEA corrosion inhibitor, the number of corrosion pits significantly decreases, and the surface becomes relatively smoother. With the addition of the SHMP corrosion inhibitor, the corrosion pits are further reduced, and the surface smoothness is significantly improved. As shown in Figure 10d–f, in an alkaline environment, the overall number of corrosion pits is significantly reduced, and under the condition with the SHMP corrosion inhibitor, the corrosion pits almost completely disappear. The morphology of the samples after rust removal further validates the mechanism of action of the corrosion inhibitors. As shown in Figure 11, under conditions without a corrosion inhibitor, corrosion causes significant damage to the substrate, and deep corrosion pits remain after rust removal. Following the addition of the PTEA corrosion inhibitor, the surface defects are significantly reduced, and the substrate structure is improved. In contrast, under the conditions with the SHMP corrosion inhibitor, especially in the alkaline environment, the sample surface is almost completely defect-free, with SHMP exhibiting the best substrate protection, further confirming the excellent performance of SHMP as a corrosion inhibitor in alkaline environments, consistent with the confocal results.

4. Analysis and Discussion

This study investigates the corrosion rate of ductile iron (DCI) under various pH conditions and with different types of inhibitors, employing electrochemical tests, including open circuit potential (OCP), polarization curves, and electrochemical impedance spectroscopy (EIS). The results demonstrate significant inhibition effects of the two inhibitors, with SHMP exhibiting higher inhibition efficiency and superior performance in alkaline environments. The corrosion inhibition mechanisms of PTEA and SHMP are analyzed below.

4.1. Corrosion Inhibition Mechanism of PTEA

PTEA is typically adsorbed onto a metal surface through molecular interactions, thereby preventing electrochemical corrosion [27,28]. Most organic compounds contain polar groups, such as nitrogen, π bonds, and double bonds, as well as non-polar groups composed of hydrogen atoms, which are essential for their role as organic corrosion inhibitors [29–32]. The adsorption of PTEA onto the Fe matrix surface is shown in Figure 12e. The lone-pair electrons of oxygen and nitrogen in PTEA interact with the Fe surface through 3D orbital interactions [33], resulting in the parallel adsorption of PTEA onto the metal surface. The active sites of PTEA are the -P=O and -NH_2 groups, which interact with metal atoms. This adsorption mode provides effective surface protection, leading to excellent corrosion inhibition by PTEA [34].

However, studies have shown that when a TEA corrosion inhibitor is added to a corrosion-prone environment, TEA preferentially adsorbs onto the graphite, thereby allowing galvanic corrosion to continue between the graphite and the substrate. When the amount of TEA is sufficiently large, excess TEA covers the graphite surface and gradually forms a protective layer over the entire DCI surface, thereby preventing galvanic corrosion between the graphite and the substrate [21].

As shown in Figure 3a, when immersed in an alkaline environment for 0 days, the DCI exhibits a clear activation process in the solution without PTEA. In contrast, when the PTEA inhibitor is present, a passivation zone forms. After soaking for 3 days (Figure 3b), the DCI again exhibits an activation process in the PTEA solution. After 10 days of immersion, as

shown in Figure 3c, no passivation process is observed in the PTEA corrosion inhibitor solution, and the i_{corr} increases compared to the values at 0 and 3 days. This is likely due to the initial adsorption of PTEA onto the surface of the ductile iron, which forms a protective film [35]. However, as the immersion time increases, aggressive ions and high temperatures increase the active sites on the DCI surface, weakening PTEA adsorption and promoting galvanic corrosion between the graphite and the steel matrix [23,36].

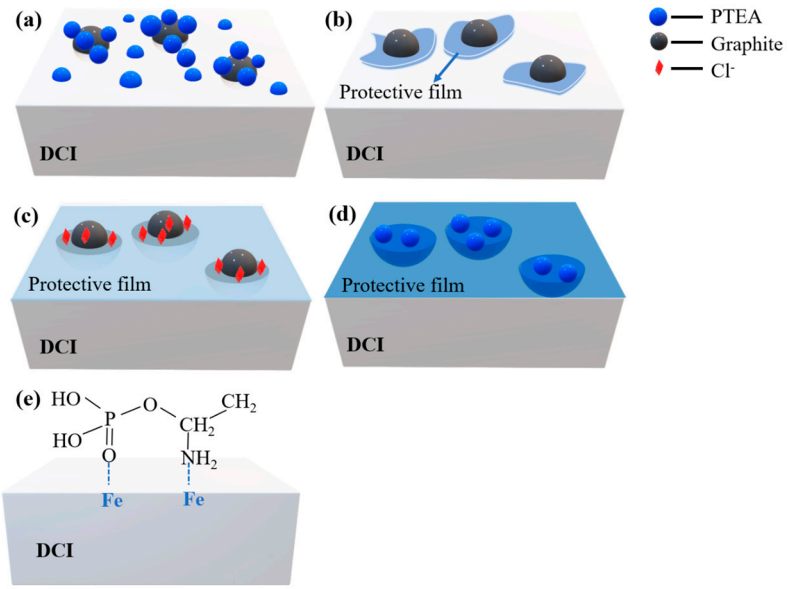


Figure 12. (**a**–**d**) Adsorption and film formation process of triethanolamine phosphate (PTEA) on surface of ductile cast iron (DCI) and (**e**) schematic diagram of adsorption interaction between PTEA and iron substrate.

Nevertheless, in the flow immersion experiment, PTEA demonstrated excellent corrosion inhibition, likely due to the continuous supply of PTEA molecules, which ensured adequate coverage of the DCI surface. As shown in Figure 7, after rust removal, graphite particles detach from the DCI surface. Furthermore, no severe pitting corrosion occurs during the 10-day immersion after the graphite particles detached. This suggests that after the detachment of the graphite, PTEA further adsorbed onto the exposed Fe matrix, hindering contact between the Fe matrix and the aggressive ions, thereby inhibiting further corrosion of the DCI [22].

Figures 5 and 6 show that the surface of the DCI undergoes uniform corrosion in a neutral environment with a corrosion inhibitor, with the corrosion pits remaining shallow. In Figure 7, whether in a neutral or alkaline environment, the weight loss corrosion rate of DCI after 120 h of immersion with the PTEA inhibitor is lower than that of the control group without the inhibitor. This is because, at a sufficient PTEA concentration, the inhibitor's protective film on the metal surface increases, isolating the metal substrate from the corrosive solution and preventing further corrosion reactions [37].

The inhibition mechanism of PTEA on DCI is illustrated in Figure 12a: PTEA is adsorbed onto the DCI surface, with a higher concentration on the graphite. In Figure 12b, due to the PTEA accumulation around the graphite, a protective film preferentially forms and expands around the graphite. In Figure 12c, the aggressive ions and high temperature increase the active sites on the DCI surface, promoting the corrosion of the DCI matrix. In Figure 12d, the graphite particles detach, and the PTEA continues to adsorb onto the Fe matrix, forming a corrosion-resistant protective film.

4.2. Corrosion Inhibition Mechanism of SHMP

The corrosion inhibition mechanism of SHMP for DCI involves polyphosphate interacting with the Fe matrix on the DCI surface to form iron polyphosphate or ferrous polyphosphate, which adsorbs onto the metal surface, thus preventing the release of Fe into the aqueous solution [17]. Upon combining with iron, the residual valence on the phosphorus–oxygen bonds forms a complex with metal ions, such as calcium, magnesium, and zinc, resulting in the formation of a stable, dense corrosion-inhibiting film on the metal surface [38]. The addition of the SHMP corrosion inhibitor causes ductile iron pipes to exhibit a clear passivation zone or trend in neutral and alkaline environments. As shown in Figure 3, the i_{corr} ratio decreases significantly compared to the case without the inhibitor. Moreover, as shown in Figure 7, SHMP exhibits the strongest corrosion inhibition effect on DCI in both alkaline and neutral environments, consistent with the electrochemical test results. This is due to the formation of a protective film when polyphosphate interacts with iron [39].

As depicted in Figure 13b, pentavalent phosphorus is surrounded by four phosphorus–oxygen tetrahedra. Polyphosphate is water-soluble and dissociates to produce 12 negatively charged oxygen atoms [40], existing as an anion in an aqueous solution. On one hand, the anion forms a cage complex with Fe^{2+}, which is adsorbed onto the cast iron surface, forming a dense corrosion-inhibiting film that prevents the anodic reaction. On the other hand, the dissociation products of SHMP can form soluble complexes with Fe^{3+}, Fe^{2+}, Na^{+}, and Ca^{2+} in solution, covering the cathode surface and providing cathodic protection [22].

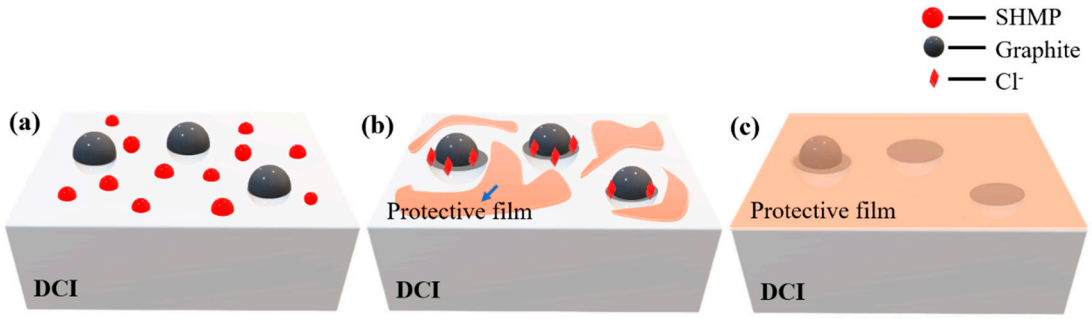


Figure 13. (**a**–**c**) Film formation and corrosion inhibition process of sodium hexametaphosphate (SHMP) on the surface of ductile cast iron (DCI).

The hydrolysis process of SHMP is as follows:

$$3(NaPO_3)_6 + 12H_2O \rightarrow 2(NaPO_3)_3 + 12NaH_2PO_4 \quad (4)$$

NaH_2PO_4 further reacts with water:

$$NaH_2PO_4 + H_2O \rightarrow NaOH + H_3PO_4 \quad (5)$$

The resulting H_3PO_4 reacts with $Fe(OH)_2$:

$$Fe(OH)_2 + 2H_3PO_4 \rightarrow Fe(H_2PO_4)_2(\text{primary iron phosphate}) + 2H_2O \quad (6)$$

$$Fe(H_2PO_4)_2 \rightarrow FeHPO_4(\text{secondary iron phosphate}) + H_3PO_4 \quad (7)$$

$$4FeHPO_4 + O_2 \rightarrow 4FePO_4(\text{terniary iron phosphate}) + 2H_2O \quad (8)$$

Among these, the primary and secondary iron phosphates are unstable in alkaline environments and easily convert to the highly stable tertiary iron phosphate, which is adhesive and insoluble. $FePO_4$ can adsorb onto a metal surface, thereby preventing the cor-

rosion process [41]. The inhibition mechanism of SHMP on DCI is illustrated in Figure 13a: SHMP hydrolyzes and generates $FePO_4$ through biochemical reactions in the presence of oxygen and a solution. In Figure 13b, $FePO_4$ is firmly adsorbed onto the DCI matrix surface and gradually expands due to its stability and adhesion. In Figure 13c, a compact $FePO_4$ corrosion-inhibiting film is formed.

4.3. Comparison Between PTEA and SHMP

While both inhibitors reduce the corrosion rate of DCI, their mechanisms differ considerably. PTEA relies on molecular adsorption to form a protective film, which may deteriorate upon prolonged exposure to aggressive environments. In contrast, SHMP forms a chemically stable precipitation layer that strongly adheres to the DCI surface, offering better long-term protection. This accounts for the superior performance of SHMP compared to PTEA, particularly in alkaline environments.

5. Conclusions

This study systematically examined the effects of the organic corrosion inhibitor PTEA and the inorganic corrosion inhibitor SHMP on the corrosion behavior of ductile cast iron (DCI) in environments with varying pH levels. The results indicate that both inhibitors exhibit significant corrosion inhibition in neutral and alkaline environments, although their inhibition mechanisms and effects differ. The key conclusions are as follows:

Both inhibitors exhibited relatively weak initial inhibition, but their performance significantly improved with prolonged immersion. SHMP demonstrated the highest performance in alkaline environments, significantly reducing the corrosion current density and enhancing corrosion resistance.

SHMP formed protective films more rapidly and stably in alkaline environments, resulting in a corrosion rate as low as 0.135 mm/a. PTEA effectively reduced corrosion in both neutral and alkaline conditions, although its effectiveness was slightly lower than that of SHMP.

PTEA functions through molecular adsorption, forming a temporary protective film that primarily inhibits cathodic reactions. In contrast, SHMP forms a stable and dense iron phosphate film, which effectively suppresses anodic reactions and provides superior corrosion protection.

The main limitation of this study lies in the need for a comprehensive understanding of the important role of SHMP and PTEA in inhibiting the corrosion of ductile iron. Future research should focus on the performance, long-term effects, and multi-dimensional exploration of the mechanisms of SHMP and PTEA corrosion inhibitors in complex environments.

Author Contributions: Conceptualization: B.W.; Methodology: B.W., C.L. and J.W.; Investigation: T.C. and L.H.; Data curation: J.L., T.C., L.H. and J.W.; Writing—original draft preparation: J.L.; Writing—review and editing: J.L. and C.L.; Supervision: J.W. and C.L.; Funding acquisition: C.L. All authors have read and agreed to the published version of the manuscript.

Funding: This study did not receive external funding or was funded by the National Natural Science Foundation of China, with the funding number being No. 52104319, and the Article Processing Charge (APC) was also funded by No. 52104319.

Data Availability Statement: The original contributions presented in this study are included in the article. For any other questions, please contact the corresponding authors.

Acknowledgments: The authors acknowledge the National Natural Science Foundation of China (No. 52104319).

Conflicts of Interest: Jing Liu and Jun Wu was employed by the company Wuhan Research Institute of Materials Protection. The remaining authors declare that the research was conducted in the absence of any commercial or financial relationships that could be construed as a potential conflict of interest.

References

1. Lee, W.H.; Wahman, D.G.; Lytle, D.A.; Pressman, J.G.; Chung, J. Microelectrode evaluation of in situ oxidant reactivity and pH variability at new ductile iron and copper coupon surfaces. *Water Res.* **2023**, *243*, 120352. [CrossRef] [PubMed]
2. Liu, M.; Du, C.; Luo, X.; Liu, C.; Wu, Z.; Li, X. Failure analysis in buried ductile iron pipelines: A study of leakage in drinking water distribution systems. *Eng. Fail. Anal.* **2023**, *151*, 107361. [CrossRef]
3. Dąbrowski, W.; Li, F. Mortar Lining as a Protective Layer for Ductile Iron Pipes. *Int. J. Civ. Eng.* **2020**, *19*, 369–380. [CrossRef]
4. Robert, D.J.; Jiang, R.; Rajeev, P.; Kodikara, J. Contribution of Cement Mortar Lining to Structural Capacity of Cast Iron Water Mains. *ACI Mater. J.* **2016**, *113*, 295–306. [CrossRef]
5. Gao, Y.; Zhang, Y.; Bi, Q. Investigation of the leaching behavior of mortar pipe lining in drinking water. *J. Wuhan Univ. Technol. Sci. Ed.* **2010**, *25*, 893–896. [CrossRef]
6. Liu, Y.; Tian, Y.; Zhang, R.; Guo, H.; Zhao, W.; Huang, J. Corrosion behavior and mechanism of ductile iron with different degrees of deterioration of cement mortar lining in reclaimed water pipelines. *RSC Adv.* **2020**, *10*, 39627–39639. [CrossRef]
7. Nguyen, V.; White, C.; Jefferson, H. Field Trial: Inspection of Cement Mortar-Lined Ductile Iron Pipe. In *Pipelines 2014: From Underground to the Forefront of Innovation and Sustainability*; ASCE Press: Reston, VA, USA, 2014; pp. 207–216.
8. Brito, V.S.; Bastos, I.N.; Costa, H.R.M. Corrosion resistance and characterization of metallic coatings deposited by thermal spray on carbon steel. *Mater. Des.* **2012**, *41*, 282–288. [CrossRef]
9. Chen, L.; Lu, D.; Zhang, Y. Organic compounds as corrosion inhibitors for carbon steel in HCl solution: A comprehensive review. *Materials* **2022**, *15*, 2023. [CrossRef]
10. Choi, Y.-S.; Shim, J.-J.; Kim, J.-G. Effects of Cr, Cu, Ni and Ca on the corrosion behavior of low carbon steel in synthetic tap water. *J. Alloy. Compd.* **2004**, *391*, 162–169. [CrossRef]
11. Negm, N.A.; Kandile, N.G.; Badr, E.A.; Mohammed, M.A. Gravimetric and electrochemical evaluation of environmentally friendly nonionic corrosion inhibitors for carbon steel in 1 M HCl. *Corros. Sci.* **2012**, *65*, 94–103. [CrossRef]
12. Lim, B.; Kim, K.; Chang, H.; Park, H.; Kim, Y. The Effect of Tungstate and Ethanolamines Added in Tap Water on Corrosion Inhibition of Ductile Cast Iron Pipe for Nuclear Power Plants. *Metals* **2020**, *10*, 1597. [CrossRef]
13. Munis, A.; Zhao, T.; Zheng, M.; Rehman, A.U.; Wang, F. A newly synthesized green corrosion inhibitor imidazoline derivative for carbon steel in 7.5% NH_4Cl solution. *Sustain. Chem. Pharm.* **2020**, *16*, 100258. [CrossRef]
14. Söylev, T.; Richardson, M. Corrosion inhibitors for steel in concrete: State-of-the-art report. *Constr. Build. Mater.* **2008**, *22*, 609–622. [CrossRef]
15. Naveen, E.; Ramnath, B.V.; Elanchezhian, C.; Nazirudeen, S.M. Influence of organic corrosion inhibitors on pickling corrosion behaviour of sinter-forged C45 steel and 2% Cu alloyed C45 steel. *J. Alloy. Compd.* **2017**, *695*, 3299–3309. [CrossRef]
16. Lekbach, Y.; Bennouna, F.; El Abed, S.; Balouiri, M.; El Azzouzi, M.; Aouniti, A.; Ibnsouda Koraichi, S. Green corrosion inhibition and adsorption behaviour of cistus ladanifer extract on 304L stainless steel in hydrochloric acid solution. *Arab. J. Sci. Eng.* **2021**, *46*, 103–113. [CrossRef]
17. Wu, G.Q. Research on the Application of Phosphate in Corrosion Inhibition Control of Water Supply Pipelines. Master's Thesis, Harbin Institute of Technology, Harbin, China, 2017.
18. Mohamed, A.; Martin, U.; Bastidas, D.M. Adsorption and Surface Analysis of Sodium Phosphate Corrosion Inhibitor on Carbon Steel in Simulated Concrete Pore Solution. *Materials* **2022**, *15*, 7429. [CrossRef]
19. Singh, A.; Ansari, K.R.; Chauhan, D.S.; Quraishi, M.A.; Lgaz, H.; Chung, I.M. Comprehensive investigation of steel corrosion inhibition at macro/micro level by ecofriendly green corrosion inhibitor in 15% HCl medium. *J. Colloid Interface Sci.* **2020**, *560*, 225–236. [CrossRef]
20. Chen, S.Q. Study on Inhibitors and Inhibition Mechanism of Aluminum Anode in Cl^--Containing Media. Master's Thesis, Harbin Institute of Technology, Harbin, China, 2012.
21. Kim, K.T.; Chang, H.Y.; Lim, B.T.; Park, H.B.; Kim, Y.S. New Mechanism on Synergistic Effect of Nitrite and Triethanolamine Addition on the Corrosion of Ductile Cast Iron. *Adv. Mater. Sci. Eng.* **2016**, *2016*, 4935602. [CrossRef]
22. Kumar, H.; Chaudhary, R.S. Influence of Sodium Hexa Metaphosphate Antiscalant on the Corrosion of Carbon Steel in Industrial Cooling Water System. *Indian J. Chem. Technol.* **2010**, *17*, 181–190.
23. Wang, B.; Liu, T.; Tao, K.; Zhu, L.; Liu, C.; Yong, X.; Cheng, X. A Study of the Mechanisms and Kinetics of the Localized Corrosion Aggravation of Ductile Iron in a Harsh Water Quality Environment. *Metals* **2022**, *12*, 2103. [CrossRef]
24. Song, Y.; Jiang, G.; Chen, Y.; Zhao, P.; Tian, Y. Effects of chloride ions on corrosion of ductile iron and carbon steel in soil environments. *Sci. Rep.* **2017**, *7*, 6865. [CrossRef] [PubMed]
25. *ASTM-G102*; Standard Practice for Calculation of Corrosion Rates and Related Information from Electrochemical Measurements. ASTM International: West Conshohocken, PA, USA, 1994.
26. Palumbo, G.; Górny, M.; Bitka, A. Influence of the Cooling Rate on Mechanical and Corrosion Properties of Ferritic Si–Mo Ductile Cast Iron. *Met. Mater. Trans. A* **2023**, *54*, 2362–2373. [CrossRef]

27. Deyab, M.A. Hydroxyethyl cellulose as efficient organic inhibitor of zinc–carbon battery corrosion in ammonium chloride solution: Electrochemical and surface morphology studies. *J. Power Sources* **2015**, *280*, 190–194. [CrossRef]
28. Nkuna, A.A.; Akpan, E.D.; Obot, I.; Verma, C.; Ebenso, E.E.; Murulana, L.C. Impact of selected ionic liquids on corrosion protection of mild steel in acidic medium: Experimental and computational studies. *J. Mol. Liq.* **2020**, *314*, 113609. [CrossRef]
29. Obot, I.B.; Macdonald, D.D.; Gasem, Z.M. Density functional theory (DFT) as a powerful tool for designing new organic corrosion inhibitors. Part 1: An overview. *Corros. Sci.* **2015**, *99*, 1–30. [CrossRef]
30. Brycki, B.E.; Kowalczyk, I.H.; Szulc, A.; Kaczerewska, O.; Pakiet, M. Organic corrosion inhibitors. *Corros. Inhib. Princ. Recent Appl.* **2018**, *3*, 33.
31. Li, H.; Zhang, Y.; Li, C.; Zhou, Z.; Nie, X.; Chen, Y.; Cao, H.; Liu, B.; Zhang, N.; Said, Z.; et al. Cutting fluid corrosion inhibitors from inorganic to organic: Progress and applications. *Korean J. Chem. Eng.* **2022**, *39*, 1107–1134. [CrossRef]
32. Ahmed, M.H.O.; Al-Amiery, A.A.; Al-Majedy, Y.K.; Kadhum, A.A.H.; Mohamad, A.B.; Gaaz, T.S. Synthesis and characterization of a novel organic corrosion inhibitor for mild steel in 1 M hydrochloric acid. *Results Phys.* **2018**, *8*, 728–733. [CrossRef]
33. Bellal, Y.; Benghanem, F.; Keraghel, S. A new corrosion inhibitor for steel rebar in concrete: Synthesis, electrochemical and theoretical studies. *J. Mol. Struct.* **2021**, *1225*, 129257. [CrossRef]
34. Shaker, L.; Al-Amiery, A.; Al-Hamid, M.A.I.; Al-Azzawi, W.K. Understanding the mechanism of organic corrosion inhibitors through density functional theory. *Koroze a Ochr. Mater.* **2024**, *68*, 9–21. [CrossRef]
35. Lee, T.H.; Tsai, J.H.; Chen, H.Y.; Huang, P.T. Polytriphenylamine and poly (styrene-co-hydroxystyrene) blends as high-performance ant icorrosion coating for iron. *Polymers* **2021**, *13*, 1629. [CrossRef] [PubMed]
36. Chen, T.; Wang, B.; Sun, L.; Liu, C.; Cheng, X.; Li, X. The coupling mechanism of shrinkage defects and graphite on the corrosion resistance of ductile iron. *Corros. Sci.* **2023**, *227*, 111798. [CrossRef]
37. Asmara, Y.P.; Herlina, F.; Sutjipto, A.G.E. Selection of Inhibitor and Recent Advances in Enhancing Corrosion Prevention. In *Defect and Diffusion Forum*; Trans Tech Publications Ltd.: Bäch, Switzerland, 2024; Volume 431, pp. 69–76.
38. Saha, G.; Kurmaih, N. The mechanism of corrosion inhibition by phosphate-based cooling system corrosion inhibitors. *Corrosion* **1986**, *42*, 233–235. [CrossRef]
39. Lata, S.; Chaudhary, R.S. Some triphosphates as corrosion inhibitors for mild steel in 3% NaCl solution. *Indian J. Chem. Technol.* **2008**, *15*, 364–374.
40. Mi, Z.L.; Zhang, X.J.; Wang, Y.; Chen, C.; Gu, J.N. Comparison of the effects of different polyphosphate dosages on controlling iron release in water distribution networks. *Water Wastewater Eng.* **2012**, *48* (Suppl. S2), 222–225. [CrossRef]
41. Girčienė, O.; Ramanauskas, R.; Burokas, V.; Martušienė, A. Formation of Phosphate Coatings on Steel and Corrosion Performance of Phosphated Specimens in Alkaline Solutions. *Trans. IMF* **2004**, *82*, 137–140. [CrossRef]

Disclaimer/Publisher's Note: The statements, opinions and data contained in all publications are solely those of the individual author(s) and contributor(s) and not of MDPI and/or the editor(s). MDPI and/or the editor(s) disclaim responsibility for any injury to people or property resulting from any ideas, methods, instructions or products referred to in the content.